Tracing the Migration History of Metal Catalysts in Metal-Assisted Chemically Etched Silicon

Firat Güder,* Yang Yang,* Umut M. Küçükbayrak, and Margit Zacharias

Laboratory for Nanotechnology, Institute of Microsystems Engineering (IMTEK), Albert-Ludwigs-University of Freiburg, Georges-Köhler-Allee 103, 79110 Freiburg, Germany

ABSTRACT Three-dimensional (3D) visualization of complex embedded nanopore networks in silicon requires expensive machinery and tedious sample preparation procedures such as electron tomography, also known as 3D transmission electron microscopy. In this article, we report a new, fast, powerful, and low-cost three-dimensional imaging technique with sub-5 nm resolution. This new imaging method is applied to metal-assisted chemically etched monocrystalline Si to demonstrate its capabilities. The AFEI (atomic layer deposition-fill-etch-imaging) technique consists of three simple process steps that are available in most material research settings. First the porous substrate is conformally coated with an atomic layer deposition (ALD) metal oxide layer. ALD is able to penetrate deep into complex, high aspect ratio pores, as it is a sequential gas-phase deposition process. Next, the cross-section of the ALD-filled porous Si substrate is etched with high-density fluorine-based plasma processing, which yields very high selectivity toward Si (*e.g.*, >400:1 for Si:ZnO). This step removes the bulk Si and exposes the metal oxide structures grown inside the pores. In the last step, the sample cross-section is examined using a standard scanning electron microscope at various angles, which allows precise imaging of hidden features and reconstruction of a 3D model of the embedded pore network.

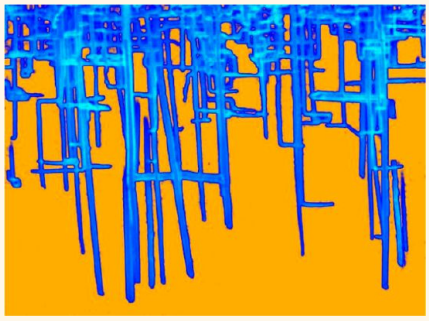

KEYWORDS: nanoporous Si · pore architecture · ALD · 3D imaging · catalytic etching

Metal-assisted chemical etching or MACE is a versatile strategy that involves wet chemical etching of Si in an HF-based aqueous solution with the help of a metal catalyst and an oxidizer.[1−3] In this fabrication regime, a Si substrate, partly covered by the metal catalyst, is submerged in an etching solution. Regions under the metal catalyst are etched faster compared to the areas that are not in direct contact with the noble metal due to accelerated oxidation of the Si surface. As a result, nanopores can be created in the substrate. Although the MACE process presents a quick and relatively low-cost alternative to the electrochemical anodization process for the fabrication of porous materials (*e.g.*, porous Si), creating highly ordered vertically oriented straight trenches is still a real challenge. Therefore, the MACE process often results in highly complex pore morphologies.

Unlike porous alumina produced by electrochemical anodization, which yields well-controlled periodically ordered pores, the shape and architecture of the created pore networks in MACE of Si can depend on several factors including the concentration of HF and oxidizing agent, type of oxidizing agent, type and morphology of the metal catalyst, etching time and temperature, illumination, substrate orientation, doping level, *etc.*[4] Until now, most of the reported conclusions about the evolution of pore networks by this method are mainly derived from top and cross-sectional scanning electron microscopy (SEM) analysis. Although a set of cross-sectional and top view SEM micrographs would be sufficient to understand the 3D microstructure of highly ordered porous materials, such as porous alumina, two-dimensional (2D) SEM data would provide no information about the etched pores extending into the bulk (third dimension). Traditionally, porous materials can be characterized by N_2 physisorption. This method provides accurate information about the pore volumes and pore sizes, but it is not able to provide information about the exact architecture of the produced nanopore networks, especially when the pores are tortuous.[5] Another technique that is capable of 3D imaging of porous materials is X-ray tomography. This technique allows

* Address correspondence to gueder@imtek.de, yang.yang@imtek.de.

Received for review November 21, 2012 and accepted January 31, 2013.

Published online January 31, 2013
10.1021/nn305413r

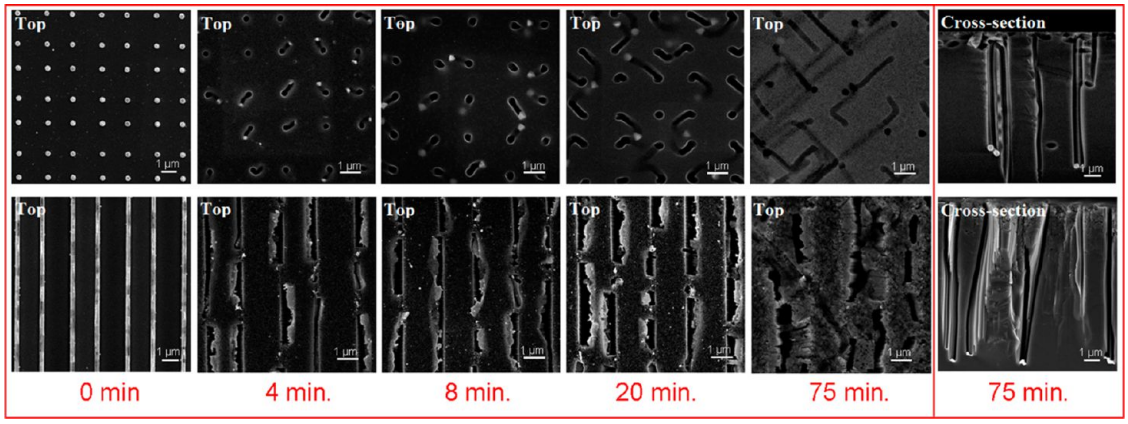

Figure 1. Time evolution of MACE of Si using patterned Ag dots and lines. After 75 min of etching, the catalysts are no longer visible from the top, and the cross-section provides little information.

visual analysis of large samples that are several hundred micrometers to millimeters in size. However, its maximum resolution is around 1 μm and at best 100 nm.[6,7] With the current technologies, the exact 3D pore architecture in nanoporous materials can be obtained only by using electron tomography, a technique that is offered by only a limited number of TEM laboratories worldwide.[8] This technique requires tedious sample preparation procedures and very expensive machinery for imaging. It is also limited in terms of the observable sample size, which is typically less than 200 nm. Therefore, a reliable imaging strategy that is capable of tracking the migration of individual particles in a three-dimensional space is still in high demand.

In this article, we report a new, low-cost, fast, and powerful 3D imaging strategy that is able to reveal the precise architecture of Si nanopore networks and the migration path of the metal catalyst produced by MACE with sub-5 nm resolution. This new strategy, which we named AFEI (atomic layer deposition-fill-etch-imaging), consists of three simple steps that can be performed in most standard Si research settings. First, the MACE-produced pores are conformally coated/filled with a metal oxide layer using the unique features of atomic layer deposition (ALD). Next, the cross-section of the Si sample is dry etched with a fluorine-based high-density plasma process. As this process etches Si much faster than the metal oxide coating (in our case ZnO) and the metal catalyst, we can obtain very high etch selectivity toward Si and induce minimal damage to the filled-in metal oxide as well as the metal catalyst. Finally, a standard SEM can be used to image the remaining 3D network of metal oxide fillings and the catalyst representing the former nanopores. By tilting the SEM stage at different angles, this technique allows us to reveal hidden features within the pore network and create 3D models of the exact architecture.

RESULTS AND DISCUSSION

In order to demonstrate the unique possibilities of the AFEI technique, we fabricated several test samples of MACE-produced porous Si. We focused mainly on patterned catalysts to isolate the etched pores with the aim of getting a clearer picture of the final pore network. In our experiments, Ag was used as the catalyst material, as it is the most studied MACE metal in the literature. The first two produced patterns consisted of isolated polycrystalline Ag dots and lines on p-type (1−20 Ω·cm) Si(100) wafers (see Supporting Information Figure S1 for the fabrication process). The patterned samples were annealed at 350 °C for 1 h in air to form tightly packed Ag clusters and to induce coarsening. The samples were then dipped into an etching solution of 50 mL of HF (wt 5%) + 0.4 mL of H_2O_2 (wt 31%) up to 75 min. At such low oxidizer concentrations, particles are expected to catalyze Si etching in crystallographically preferred ⟨100⟩ directions (*i.e.*, anistropically).[4] Figure 1 shows a series of top and cross-sectional SEM images displaying the pore evolution during the MACE process. Although particle movement can be easily tracked in the initial stages of the etching process with standard SEM imaging, after approximately 20 min, dots and lines start to penetrate deeper into the Si substrate. After this point the catalyst particles cannot be tracked accurately, neither from the top nor from the cross-section of the sample. This limits the possibility of making definitive conclusions about the 3D architecture of the etched pore network *via* migration of a Ag catalyst. Therefore, an alternative approach is required to visualize the hierarchy of the internal network.

Figure 2 illustrates the AFEI technique schematically. The most important step in this imaging strategy is the conformal deposition of metal oxides into high aspect ratio nanoscale pores by ALD. ALD is a sequential chemical vapor deposition (CVD) technique that replaces the continuous gas reactions in conventional CVD processes with two half surface reactions, enabling conformal deposition of a large variety of oxide, nitride, sulfide, *etc.*, thin films with monolayer precision in deep pores and over complex 3D structures in a wide temperature window.[9] Here, we used diethylzinc and H_2O as the precursor pair at 150 °C for the deposition of a 100 nm ZnO layer into MACE-produced pores. This

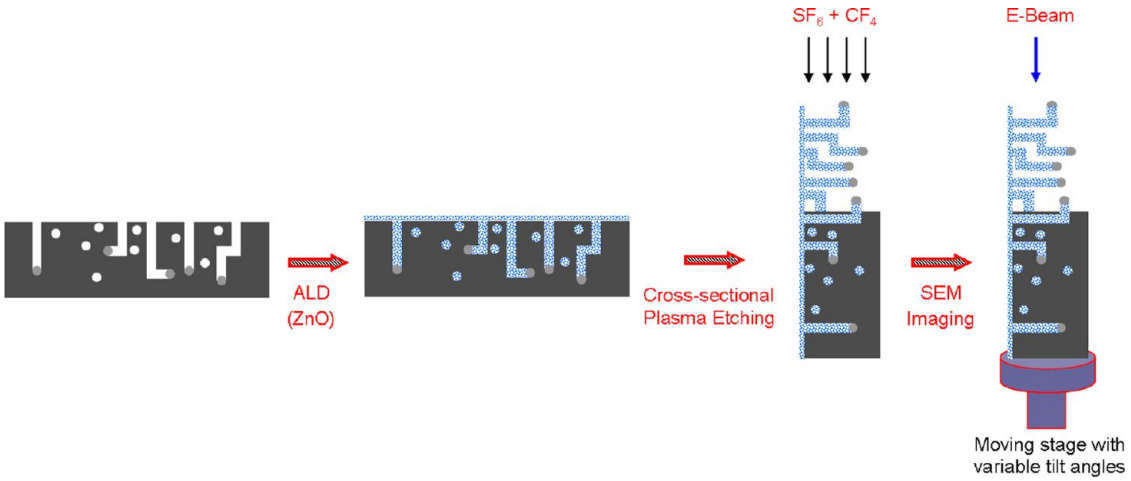

Figure 2. Schematic illustration of the AFEI (atomic layer deposition-fill-etch-imaging) technique.

step is similar to the fabrication of nanotubes and nanowires using the template-based synthesis approach with ALD coatings.[10−13] In our case, ideally all the pores with small diameters (<200 nm) can be completely filled, while those with large diameters (>200 nm) are partly filled, forming tubular structures. ZnO was used as the ALD filling material due to two important factors: (1) Si yields high selectivity with respect to ZnO when etched with a fluorine-based high-density plasma process (>400:1) and (2) ZnO is an electrically conductive metal oxide, which is very important for high-resolution SEM imaging (minimal charging when subjected to the e-beam). ALD-filled samples were then cleaved, and the cross-section was etched in an inductively coupled plasma (ICP) etcher with a mixture of SF_6 (40 sccm) and C_4F_8 (70 sccm) gases. After this process, the embedded pore network is completely exposed outside which can be imaged with a high-resolution SEM with sub-5 nm resolution (Figure S2). Please note that silicon, unlike porous alumina or soft templates, cannot easily be etched away using a wet acidic solution (*e.g.*, phosphoric acid) or combusted away by annealing in air, respectively. Wet chemical etching of Si is commonly achieved by using either KOH or TMAH or a mixture containing HNO_3 and HF, all of which would dissolve the ALD-deposited ZnO and even etch the metal catalyst. In addition, ALD-deposited high aspect ratio ultrathin nanotubes/nanowires with diameters on the order of a few nanometers could never survive the harsh wet chemical etching process due to their low mechanical stability. Therefore, a carefully optimized high-selectivity plasma process is needed in order to retain the fragile ZnO structures and also to protect the metal catalyst embedded in the bulk.

A selection of pore architectures produced by the patterned Ag dot and line arrays is presented in Figure 3. Upon AFEI, while dot arrays with bigger polycrystalline dots (~450 nm) seemed to have etched straight into the Si substrate, smaller polycrystalline Ag dots (~200 nm) etched curvy and helical pores (Figure 3 and Figure S3). This result shows that the number of grains in an isolated silver dot can make a huge difference in the etch morphology. Another interesting point is that the top portion of the Si substrate seems to be considerably more porous after MACE. This could be due to dissolution and redeposition of small Ag particles from the dots on the substrate, which continue etching when in contact with the substrate. We also observed that small particles can even break away from the Ag dots while deep in the substrate, forming some smaller branches off the side of the bigger pores. When we look at the line patterns using AFEI perpendicular to the lines, it appears that the lines etch mostly vertically into the substrate. However, when we examine the substrate pore architecture parallel to the line patterns, we see that the lines often break and move in different directions including parallel to the substrate surface. They can also disintegrate into smaller pieces and create a disordered pore network.

In a third demonstration experiment, we deposited isolated single-crystalline Ag particles onto a Si surface using patterned photoresist holes through the well-known electroless plating process with a mixture of $AgNO_3$, water, and HF under standard room lighting.[14,15] The prepared salt solution is acidic; therefore it does not attack the base-soluble photoresist layer, allowing easy deposition of patterned particle groups. The fabrication process for this sample can be seen in Figure S4. Figure 4a shows an SEM micrograph of the patterned isolated single-crystalline Ag particle groups on the Si surface. The prepared sample was dipped into the etching solution for 75 min and subsequently coated with 30 nm of ALD ZnO. A cross-sectional image of the MACE-processed and ALD-coated sample can be seen in Figure 4b. The embedded network of pores is revealed with high accuracy (Figure 4c) after cross-sectional ICP etching with the same recipe as described above. Here, the clear advantage of the AFEI technique compared to standard SEM imaging can be seen (Figure 4b *vs* Figure 4c). We then

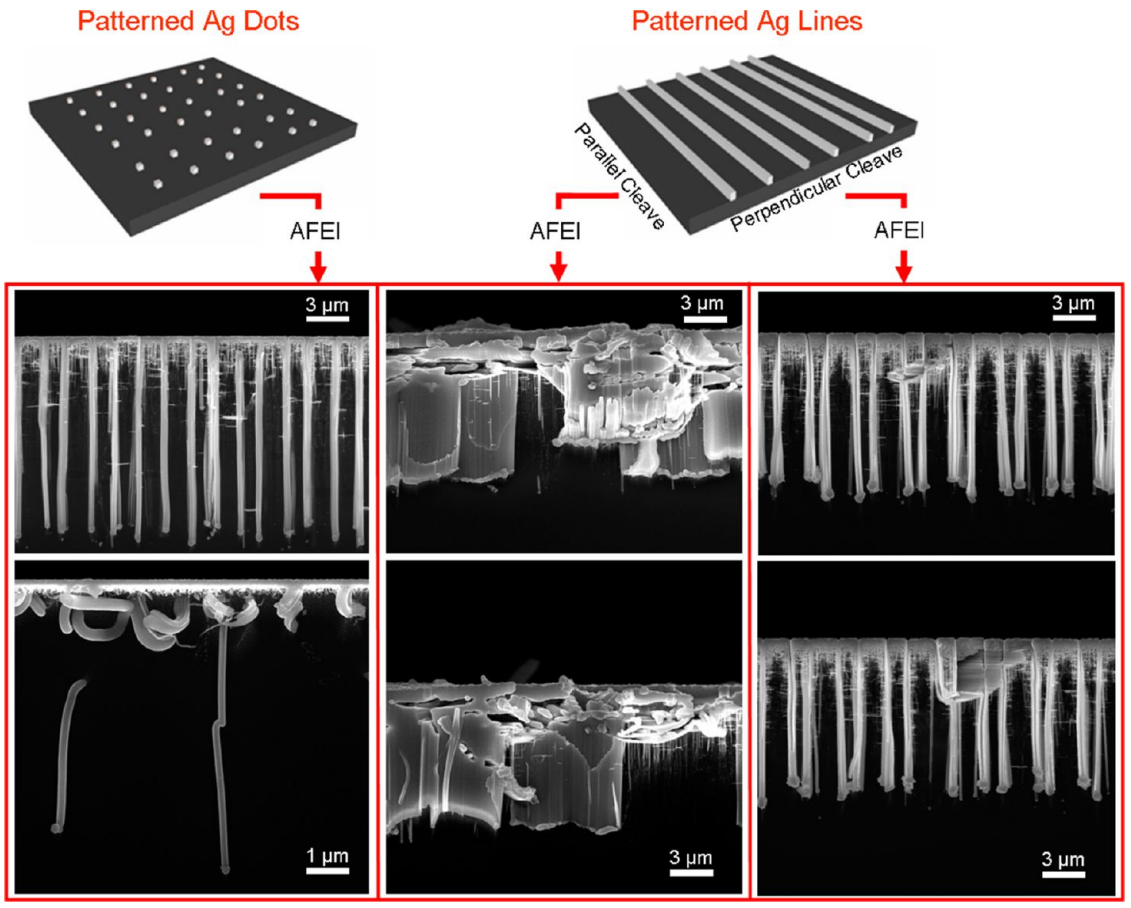

Figure 3. Cross-sectional AFEI analysis of MACE-produced porous Si using patterned catalysts. Using AFEI all aspects of the pore network can be revealed.

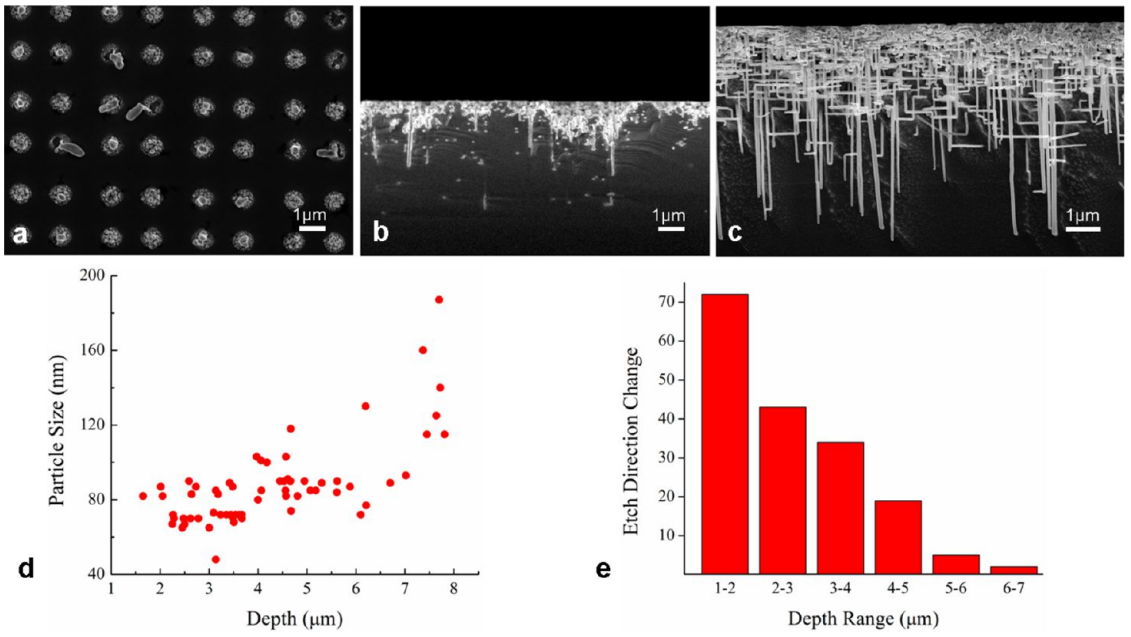

Figure 4. (a) Patterened Ag particle groups; (b) cross-sectional SEM image of ALD ZnO-coated MACEd sample from (a); (c) sample cross-section after plasma etching and the completed AFEI procedure; graph displaying the relationship between (d) particle size and etch depth; and (e) number of changes in the etch direction and depth range induced by MACE.

investigated the relationship between particle size and etch depth in the MACE process. The resulting data can be seen in Figure 4d. Because of the high porosity observed in the near-surface region (down to a depth

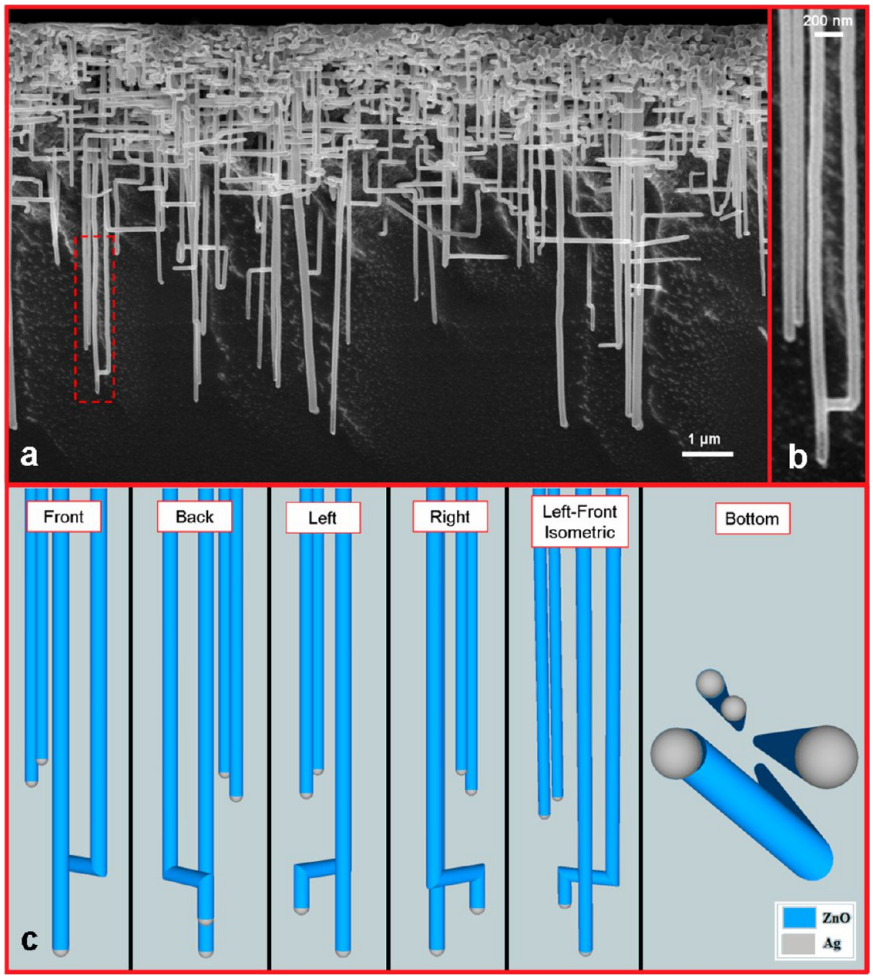

Figure 5. (a) AFEI analysis of MACEd sample using patterned Ag particle groups; (b) zoomed-in view of the marked area shown in (a); (c) 3D reconstruction of the pore architecture shown in (b) from various viewpoints.

of approximately 1.5 μm), we were not able to make size measurements in this part. Therefore, no data point is present in this interval in the graph. Although particles of <90 nm could be found at all depth ranges, larger particles (>140 nm) could be observed only at higher depths. This shows that, contrary to what is expected, both smaller and bigger particles can etch into the Si substrate at the same speed since both smaller and bigger particles can be found in the deepest trenches. This phenomenon could never be observed before using only standard cross-sectional SEM imaging. We also wanted to understand why larger particles are not observed at the lower depth ranges, although both bigger and smaller particles seem to etch Si at the same speed. We counted the number of jumps in the etching direction in a given depth range (Figure 4e). It can be seen that as the particles etch deeper into the substrate, they change their etching direction less frequently. When this result is correlated with the particle size/etch depth data shown in Figure 4d, it can be concluded that smaller particles change their etching direction more often than that of bigger particles. This is the reason that bigger particles always etch deeper trenches and only some of the smaller particles etch as deep trenches as the bigger particles since they lose a fair amount of time changing their etching direction and etching in nonvertical ⟨100⟩ directions. One other implication of this analysis is that as fewer numbers of overall particles penetrate to higher depths, the porosity changes across the cross-section of the sample and is not constant everywhere. Thus, the pore density is inversely related to depth, meaning higher porosity at lower depths and lower porosity at high depths.

Tsujino and Matsumura studied the effect of Ag particle shape on the MACE of Si(100) and concluded that spherical Ag particles were responsible for vertical and cylindrical holes in Si where faceted particles were responsible for changes in the etching course in one of the ⟨100⟩ directions.[16] The above authors also mentioned that most particles eventually become spherical after long time etching due to partial etching of the Ag catalyst surface in the etching solution, hence, eventually etching straight pores. This explanation somewhat contradicts our direct observation made with the AFEI technique. It is known that larger crystals show more obvious crystal facets than smaller crystals. However, as seen in our AFEI results, it is clear that the

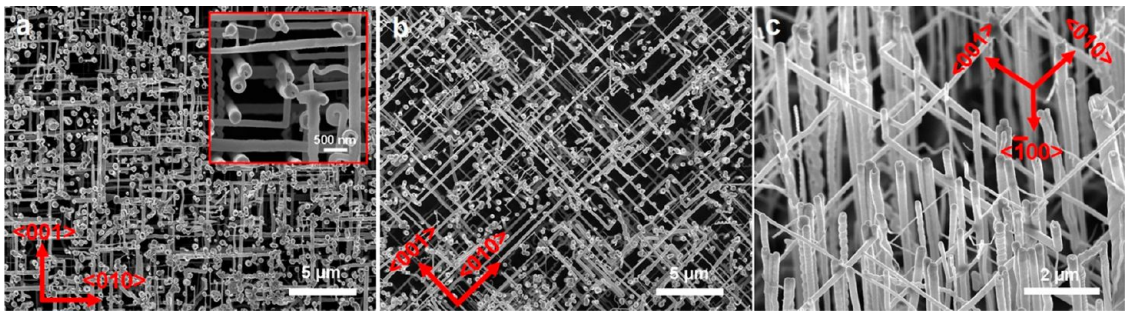

Figure 6. (a) High-density, self-supporting, oriented nanowire/nanotube network; (b) reduced density version of the nanowire network shown in (a); (c) 45°-tilted view of the structures shown in (b).

straight etching process occurs throughout the MACE process for the larger particles and not only in the later stages. Although it is not completely clear, well-faceted particles appear to etch straight pores better than spherical particles, contrary to what was reported before. The reason for this may be the fact that the bottom surfaces of the faceted crystals are in better contact with the surface of the initially flat Si substrate, catalyzing etching in only one direction. When the particles are smaller, *i.e*, more spherical, their etch direction becomes more stochastic.

We have exploited the unique capabilities of AFEI for advanced 3D imaging and modeling of pore networks produced by MACE of single-crystalline Si. Accurate 3D imaging and modeling of the pore networks can easily be achieved by tilting the sample stage during SEM analysis at various angles. This allows more detailed SEM analysis to be performed, capturing information about the three-dimensional nature of the fabricated pores and revealing hidden pore features that are otherwise not visible. Once SEM micrographs at several tilt angles are captured, a 3D model can be created either by a commercially available 3D image reconstruction software package or simply by hand using computer-aided engineering drawing tools and the obtained SEM data. Figure 5a shows an SEM image of a pore network obtained by AFEI. Here, the goal was to create a 3D reconstruction of the area marked in red to reveal the exact architecture of the etched pores and expose hidden trenches. A magnified version of the marked area is shown in Figure 5b. A series of SEM micrographs of the sample were captured when the sample was tilted sideways at 0°, 20°, 35°, 45° and −20°, −35°, −45° tilt angles. In addition, the sample was also tilted 45° forward to image the bottom of sample. The tilting procedure is shown in more detail in Figure S5. Tilting and imaging at these angles provide enough information to create an accurate 3D model of the area of interest. Next, Google Sketchup,[17] a widely available engineering drawing program, was used to reconstruct a 3D model of the pore network. The results are presented in Figure 5c. In this model, it becomes clear that one of the pores is actually extending behind another pore, which was not visible in simple 2D cross-sectional SEM analysis. Using the created model, this hidden structure can be visualized from different perspectives, showing the precise architecture of the pore network in the marked area. An animation, displaying a 360° view of the reconstructed model, has been created. The movie can be seen in Supporting Information Movie S6. This movie once again displays the unique capabilities of the AFEI strategy.

Although the AFEI process is a powerful tool for imaging, its application is not limited by that. AFEI can also be used as a fabrication tool especially for the synthesis of self-supported, size and density tunable, highly oriented three-dimensional nanotube/nanowire networks (NNNs) on silicon. There have been several reports on the fabrication of three-dimensional nanotube and nanowire networks in the literature.[18−20] Rauber *et al*. was able to produce highly oriented NNNs using ion track etched polymer membranes and electrochemical deposition.[20] In their approach, the polymer membrane was dissolved in an organic solvent, leaving behind the nanowire network. However, their technique was limited by inherit restrictions of mass transport for solution-based electrochemical deposition, which prevented very small pores to be filled completely (smallest deposited nanowire diameter ∼35 nm). In addition, fabrication of nanotube networks was not possible due to solution-based removal of the polymer support, which destroyed these highly fragile nanostructures. The ZnO NNNs produced by AFEI can be seen in Figure 6. As shown before, we often observe a highly porous layer in the top few micrometers of the Si substrate after MACE. In order to gain access to the NNN from the top, we polished off the top layer (∼2 μm), following ALD deposition, by chemical mechanical polishing (CMP). After this we carried out the usual ICP etching step. The highly dense NNNs can be seen in Figure 6a. The density of the NNNs can be tuned either by adjusting the Ag deposition conditions to increase or decrease the number of particles deposited during electroless plating or by removing a thicker top layer *via* CMP. As mentioned previously, pore density is reduced as we go from the top of the sample to the bottom. Therefore, when a thicker layer is removed from the top *via* CMP, the high-density areas can be cleared. Figure 6b and c

show a lower density NNN produced by removing a thicker layer from the top.

CONCLUSIONS

In summary, a new, fast, powerful, and low-cost three-dimensional imaging technique with sub-5 nm resolution has been developed. This new technique, called AFEI, combines ALD and plasma-based Si etching to reveal details of embedded pore networks in porous Si produced by the MACE process. Using the AFEI technique, the following new conclusions about the MACE process can be drawn from first, direct observations:

- While polycrystalline Ag dots with bigger diameters (~450 nm) etched straight pores into the Si substrate, smaller dots (~200 nm) etched curvy and helical pores. This result shows that the number of grains in a cluster has a large influence on the etch morphology for polycrystalline dots, most probably due to the coupling effect.
- Polycrystalline Ag lines can break during etching and move in different horizontal directions. Therefore it is not possible to etch long and deep vertical trenches.
- Both bigger (>140 nm) and smaller (<90 nm) single-crystalline Ag particles catalyze Si etching approximately at the same speed.
- Smaller particles change their etching course in equivalent Si⟨100⟩ directions more frequently than bigger particles. This is contrary to the previously proposed hypothesis that crystal facets are the main reason for the changes in the etching direction, as bigger particles have more obvious crystal facets.

In conclusion, we demonstrated that the AFEI strategy is an excellent tool for 3D visualization and accurate statistical analysis of embedded pore architectures. By obtaining respective SEM images at various tilt angles, 3D models of the pore architecture can be created. These models can be used in revealing hidden features in the pore network. The AFEI technique is a general imaging strategy and is expected to work with other porous materials given that ALD materials with high etch selectivity to the given porous material are present as well as highly selective and carefully optimized plasma etching recipes. The self-supported tunable nanowire/nanotube networks are suitable for many applications including catalysis, energy conversion, sensing, *etc.*

EXPERIMENTAL METHODS

Fabrication of Patterned Ag Polycrystalline Dots and Lines. A 600 nm Ag layer thermally evaporated on a virgin Si(100) wafer using source pellets with 99.99% purity provided by Kurt J. Lesker Company at a pressure of approximately 4×10^{-5} mbar. The evaporated layer is then turned into dots and lines by patterning and an AZ5214 E-type photoresist (MicroChemicals) using single and double exposure near-field phase shift lithography (see Figure S1) and structured using plasma etching for 5 min with 50 sccm of Ar and 150 W platen power at a pressure of about 23 mTorr. After film structuring, the remaining photoresist is removed by O_2 plasma and an acetone dip.

Ag Catalyst Coarsening by Thermal Annealing. Fabricated polycrystalline Ag dot and line patterns are annealed at 350 °C for 1 h in air in a conventional high-temperature box furnace manufactured by Carbolite.

Deposition of Patterned Ag Particle Groups. Photoresist hole patterns were fabricated once again using near-field phase shift lithography and an AZ5214 E-type photoresist. However, this time the photoresist was subjected to reversal bake after the second exposure to create photoresist holes instead of dots. The Si sample with the patterned photoresist holes was dipped into a solution consisting of 5.1 mL of HF (wt 5%) + 195 mL of H_2O + 0.061 g of $AgNO_3$ (Sigma Aldrich, 99.9999) for 20 s under standard lighting to deposit small crystallites (40−200 nm in diameter) into exposed Si areas. After the deposition, the resist is removed by an acetone dip.

Metal-Assisted Chemical Etching of Si. Si(100) samples with the patterned catalysts were dipped into a solution of 50 mL of HF (wt 5%) and 0.4 mL (wt 31%) of H_2O_2 for varying durations up to 75 min under standard room lighting conditions.

Atomic Layer Deposition of ZnO. MACEd Si samples were coated by ZnO using diethylzinc and water as precursors at 150 °C in a vertical flow type hot wall reactor (OpAL, Oxford Instruments). Before deposition, the reactor was pumped to 20 mTorr and kept between 170 and 190 mTorr during the process. N_2 was used as the purge gas to remove unreacted species and the reaction byproducts from the reaction environment to prevent parasitic CVD reactions. The thickness of the ZnO layer could be adjusted by increasing or decreasing the number of deposition cycles. In order to allow sufficient penetration of the precursors into the high aspect ratio deep pores, the pump line was flooded with 400 sccm of N_2 for 10 s after each precursor pulse. Flooding the vacuum line with N_2 reduces the pumping speed and therefore allows longer exposure times before the reactor is purged. For a 4 in. wafer with a 3.5 × 3.5 cm porous area, an exposure time of 10 s was experimentally determined to be sufficient to create conformal ALD coatings for aspect ratios of up to 300.

Fluorine-Based Inductively Coupled Plasma Etching of Si. ZnO-coated MACEd samples were cleaved, and the cross sections were etched in an ICP etcher manufactured by STS using a gas mixture of 70 sccm C_4F_8 and 40 sccm SF6 at 12 and 600 W platen and coil power, respectively. While the Si etch rate is approximately 1 μm/min with this recipe, the ZnO etch rate was so slow that it was not detectable. A 30 nm ZnO layer remained almost intact after 6 μm of Si etching. Therefore, expected etch selectivity should be greater than at least 400.

Scanning Electron Microscopy Analysis and 3D Modeling. The revealed pore network was investigated using a high-resolution scanning electron microscope (Nova NanoSEM) manufactured by FEI with a nominal maximum resolution of 1 nm. The SEM was equipped with a tiltable *x-y-z* moving stage, which was used for detailed 3D analysis of the pore architecture. The obtained SEM data were used for the construction of a 3D model of the network using the Google SketchUp software package, which is available online at http://sketchup.google.com/ free of charge.

Chemical Mechanical Polishing. The porous top layer from the Si substrate was removed using a TegraForce-1 chemical mechanical polishing tool manufactured by Struers. The substrate was lapped with only water on a SiC grinding film with 5 μm grain size at 40 rpm under 50 N applied force of varying durations.

Conflict of Interest: The authors declare no competing financial interest.

Acknowledgment. We would like to thank the German Research Foundation (DFG) for financial support (ZA 191/24-1)

and Armin Baur, Michael Reichel, and the IMTEK cleanroom staff for their assistance in the experiments.

Supporting Information Available: Additional images and a movie file are available. This material is available free of charge *via* the Internet at http://pubs.acs.org.

REFERENCES AND NOTES

1. Li, X.; Bohn, P. W. Metal-Asisted Cemical Eching in HF/H_2O_2 Produces Porous Silicon. *Appl. Phys. Lett.* **2000**, *77*, 2572–2574.
2. Peng, K. Q.; Yan, Y. J.; Gao, S. P.; Zhu, J. Dendrite-Assisted Growth of Silicon Nanowires in Electroless Metal Deposition. *Adv. Funct. Mater.* **2003**, *13*, 127–132.
3. Sailor, M. J. *Porous Silicon in Practice*; Wiley-VCH Verlag & Co.: Weinheim, 2012.
4. Huang, Z.; Geyer, N.; Werner, P.; de Boor, J.; Goesele, U. Metal-Assisted Chemical Etching of Silicon: a Review. *Adv. Mater.* **2011**, *23*, 285–308.
5. Groen, J. C.; Peffer, L. A. A.; Perez-Ramirez, J. Pore Size Determination in Modified Micro- and Mesoporous Materials. Pitfalls and Limitations in Gas Adsorption Data Analysis J. *Microporous Mesaporous Mater.* **2003**, *60*, 1–17.
6. Haddad, W. S.; McNulty, I.; Trebes, J. E.; Anderson, E. H.; Levesque, R. A.; Yang, L. Ultrahigh-Resolution X-ray Tomography. *Science* **1994**, *266*, 1213–1215.
7. Dierolf, M.; Menzel, A.; Thibault, P.; Schneider, P.; Kewish, C. M.; Wepf, R.; Bunk, O.; Pfeiffer, F. Ptychographic X-Ray Computed Tomography at the Nanoscale. *Nature* **2010**, *467*, 436–439.
8. Zecevic, J.; Gommes, C. J.; Friedrich, H.; de Jongh, P. E.; de Jong, K. P. Quantification of Mesoporosity of Zeolite Y – Electron Tomography Study. *Angew. Chem., Int Ed* **2012**, *51*, 4213–4217.
9. Knez, M.; Nielsch, K.; Niinistö, L. Synthesis and Surface Engineering of Complex Nanostructures by Atomic Layer Deposition. *Adv. Mater.* **2007**, *19*, 3425–3438.
10. Subannajui, K.; Güder, F.; Danhof, J.; Menzel, A.; Yang, Y.; Kirste, L.; Wang, C.; Cimalla, V.; Schwarz, U.; Zacharias, M. An Advanced Fabrication Method of Highly Ordered ZnO Nanowire Arrays on Silicon Substrates by Atomic Layer Deposition. *Nanotechnology* **2012**, *23*, 235607.
11. Perez, I.; Robertson, E.; Banerjee, P.; Henn-Lecordier, L.; Son, S. J.; Lee, S. B.; Rubloff, G. W. TEM-Based Metrology for HfO_2 Layers and Nanotubes Formed in Anodic Aluminum Oxide Nanopore Structures. *Small* **2008**, *4*, 1223–1232.
12. Zierold, R.; Wu, Z.; Biskupek, J.; Kaiser, U.; Bachmann, J.; Krill, C. E.; Nielsch, K. Magnetic, Multilayered Nanotubes of Low Aspect Ratios for Liquid Suspensions. *Adv. Funct. Mater.* **2011**, *21*, 226–232.
13. Chong, Y. T.; Yau, M. Y.; Yang, Y.; Zacharias, M.; Gortlitz, D.; Nielsch, K.; Bachmann, J. Superparamagnetic Behavior in Cobalt Iron Oxide Nanotube Arrays by Atomic Layer Deposition. *J. Appl. Phys.* **2011**, *110*, 043930.
14. Mallory, G. O.; Hajdu, J. B. *Electroless Plating: Fundamentals and Applications*; Noyes Publications/William Andrew Publishing: Norwich, 1990.
15. Sayed, S. Y.; Daly, B.; Buriak, J. M. Characterization of the Interface of Gold and Silver Nanostructures on InP and GaAs Synthesized via Galvanic Displacement. *J. Phys. Chem. C* **2008**, *112*, 12291–12298.
16. Tsujino, K.; Matsumura, M. Boring Deep Cylindrical Nanoholes in Silicon Using Silver Nanoparticles as a Catalyst. *Adv. Mater.* **2005**, *17*, 1045–1047.
17. Google SketchUp can be downloaded free of cost at http://sketchup.google.com/.
18. Cao, X.; Xie, Y.; Li, L. Spontaneous Organization of Three-Dimensionally Packed Trigonal Selenium Microspheres into Large-Area Nanowire Networks. *Adv. Mater.* **2003**, *15*, 1914–1918.
19. Wang, W.; Tian, M.; Abdulagatov, A.; George, S. M.; Lee, Y.-C.; Yang, R. Three-Dimensional Ni/TiO_2 Nanowire Network for High Areal Capacity Lithium Ion Microbattery Applications. *Nano Lett.* **2012**, *12*, 655–660.
20. Rauber, M.; Alber, I.; Müller, S.; Neumann, R.; Picht, O.; Roth, C.; Schökel, A.; Toimil-Molares, M. E.; Ensinger, W. Highly-Ordered Supportless Three-Dimensional Nanowire Networks with Tunable Complexity and Interwire Connectivity for Device Integration. *Nano Lett.* **2011**, *11*, 2304–2310.